Ceramics International xxx (xxxx) xxx

Contents lists available at ScienceDirect

Ceramics International

journal homepage: www.elsevier.com/locate/ceramint

Novel ZnO-biochar nanocomposites obtained by hydrothermal method in extracts of *Ulva lactuca* collected from Black Sea

Anca Dumbrava [a,*], Cristian Matei [b], Aurel Diacon [c], Florin Moscalu [d], Daniela Berger [b,**]

[a] Ovidius University of Constanta, Department of Chemistry and Chemical Engineering, 124 Mamaia Blvd., Constanta, 900527, Romania
[b] University Politehnica of Bucharest, Department of Inorganic Chemistry, Physical Chemistry and Electrochemistry, 1-7 Polizu Street, Bucharest, 011061, Romania
[c] University Politehnica of Bucharest, Department of Bioresources and Polymer Science, 1-7 Polizu Street, Bucharest, 011061, Romania
[d] Ovidius University of Constanta, Department of Physics, 124 Mamaia Blvd., Constanta, 900527, Romania

ARTICLE INFO

Keywords:
ZnO@C nanocomposite
Capped zinc oxide
Green synthesis
Ulva lactuca
Photocatalytic properties
Wastewater treatment

ABSTRACT

The aqueous extract of *Ulva lactuca*, obtained from algae waste, has been used both as precursor for nanobiochar and source of phycocolloids, for obtaining of ZnO@C composites by hydrothermal method, through two synthesis routes, and capped ZnO nanopowders. The nanomaterials were characterized by XRD, SEM, thermal analysis, UV–vis, PL and FTIR spectroscopy. The presence of ZnO with hexagonal wurtzite structure was confirmed by XRD, while the presence of biochar and capping molecules was confirmed by FTIR spectroscopy and thermal analysis correlated with the total organic carbon determination. The band gap energy was calculated from diffuse reflectance spectra. The photocatalytic properties were tested in the degradation of Congo red azo dye under UV and visible light irradiations, the prepared zinc oxide-biochair nanocomposites demonstrating a good photocatalytic activity, superior to the pristine ZnO nanopowders obtained in similar conditions. The results confirmed a good fit with the Langmuir–Hinshelwood kinetic model. A correlation between photoluminescent and photocatalytic properties of nanomaterials was done. The properties of ZnO@C nanocomposites depended on the synthesis route were compared with those of capped and pristine ZnO samples.

1. Introduction

Zinc oxide (ZnO), a II-VI direct wide band gap (3.37 eV) semiconductor with a large excitation binding energy (60 meV), has many properties which make it an indispensable material in practice, with applications in electronics, photocatalysis, solar cells, medicine, etc. [1–3]. As photocatalyst, ZnO has been increasingly studied in recent years mainly due to several advantages like its abundance, availability, low toxicity and production cost. An additional argument for using ZnO as a photocatalyst, especially in the wastewater treatment, consists in its antibacterial and antifouling properties [4]. Furthermore, the photocatalytic activity of ZnO nanopowder can be tuned by synthesis method, together with the particles dimension and morphology [2,5,6]. Hence, several strategies have been proposed in order to enhance the photocatalytic activity of ZnO, as the metal/non-metal doping for decreasing the band gap, coupling of nanocarbon with ZnO@C composite formation, crystal growth and shape control, or the surface modification [4]. The ZnO surface modification is an approach consisting in capping of ZnO nanoparticles with synthetic [7,8] or natural organic molecules. Recently, the utilization of biomolecules as a template has been intensively studied, with the emerge of the new field of biotechnology. ZnO is indeed widely obtained using green chemistry and biotechnologies, being involved various natural sources [9–12].

Also, the synthesis of ZnO-based composites consists of a strategy which involves the combination between ZnO and other materials for obtaining new materials with improved properties. For instance, since nanoparticles are prone to be agglomerated in large clusters, resulting in the dispersibility loss and decrease of the reaction activity, materials such as carbon or silver have been considered for supporting nanoparticles [13]. To optimize the photocatalytic performance of ZnO, various carbonaceous materials have been used to obtain ZnO@C composites. The advantages of carbon materials consist in a high surface area, which may improve the adsorption capacity of ZnO and the increase light absorption, and a stable structure [3,13]. Moreover, the photocatalytic performance can be enhanced by the heterojunction composed of metal oxide and carbon, which reduces the recombination

* Corresponding author.
** Corresponding author.
E-mail addresses: adumbrava@univ-ovidius.ro (A. Dumbrava), daniela.berger@upb.ro (D. Berger).

https://doi.org/10.1016/j.ceramint.2022.11.178
Received 16 August 2022; Received in revised form 17 October 2022; Accepted 14 November 2022
Available online 18 November 2022
0272-8842/© 2022 Published by Elsevier Ltd.

Please cite this article as: Anca Dumbrava, *Ceramics International*, https://doi.org/10.1016/j.ceramint.2022.11.178

efficiency of photogenerated carriers [14,15]. Among carbon materials, the biochar, a carbon-rich material which is mainly produced through the biomass thermal decomposition in a limited oxygen environment, but also by other thermo-chemical processes like hydrothermal liquefaction, gasification, torrefaction and direct combustion, has gained increasing importance in recent years [16,17]. The solvothermal process is another route for obtaining biochar and nanobiochar, being an energy-saving and environmentally friendly process. The most used carbon sources for obtaining biochar nanocomposites are glucose, starch, and commercially available cellulose, but, for large-scale preparation, it is not practical to use these high purity organic compounds [13].

In our study, we aimed to obtain ZnO@C nanocomposite by using natural compounds from seaweed as carbon source. We chose *Ulva lactuca* (sea lettuce) as a source of polysaccharides; the polysaccharides are associated with the cell wall and intercellular spaces of the seaweed species (like alginate, carrageenan, and agar), which belong to the phycocolloids class, having many applications [18,19]. In the *Ulva lactuca* composition, the carbohydrates represent approximately 53%, including cell-wall water-soluble sulfated ulvan, alkali-soluble hemicellulosic β(1,4)-D-glucuronan and β(1,4)-D-glucoxylan, and amorphous α-cellulose with xylose residues [20]. As a water-soluble polysaccharide, ulvan can be efficiently extracted in water from green seaweeds [21–24]. The algal biochar obtained by several methods demonstrated performance for use as supercapacitors, pollutants and CO_2 adsorbents, due to its graphitic carbon structure, high electron transport, and specific surface area [17].

We used the aqueous extract of *Ulva lactuca* waste to obtain biochar by the hydrothermal method. Compared to the use of algal mass as a raw material for biochar, the proposed method have the advantage of obtaining low dimension biochar particles. As well, the thermal stable biomolecules are preserved in the aqueous extract and can influence the subsequent synthesis. ZnO-based nanocomposites were synthesized both in as-obtained biochar suspension and in *Ulva lactuca* aqueous extracts, by hydrothermal method, varying the synthesis parameters. We used the seaweeds extract as template and also as a carbon source for nanobiochar, following two different strategies for the modification of ZnO surface. The properties of as-obtained ZnO-based nanopowders were compared with those of pristine ZnO and ZnO obtained in the *Ulva lactuca* extract.

2. Experimental

2.1. Materials

The reagents of high purity were obtained from Sigma-Aldrich (zinc acetate, $Zn(CH_3COO)_2{\cdot}2H_2O$; Congo red, disodium salt of 3,3′-([1,1′-biphenyl]-4,4′-diyl)bis(4-aminonaphthalene-1-sulfonic acid), $C_{32}H_{22}N_6Na_2O_6S_2$) and Loba Chemie (sodium hydroxide, NaOH), and were used as received, without further purification. The green seaweeds waste was collected from the beach of Black Sea south coast, Constanta County, in June 2021.

2.2. Synthesis of ZnO-based nanopowders

We obtained ZnO@C nanocomposites by hydrothermal synthesis in *Ulva lactuca* extract. To study the influence of the seaweeds extract during the oxide synthesis, we also obtained ZnO nanopowders in the same extract by both hydrothermal method and chemical precipitation, and for comparison, pristine ZnO nanopowders were synthesized by replacement of the extract with water.

Ulva lactuca extract (ULE). The *Ulva lactuca* seaweeds were washed, dried and kept as a powder (ULP), as we previously reported [25,26]. ULP and water were mixed in a ratio of 1 g ULP: 100 mL H_2O and magnetically stirred for 2 h at 60 °C. The solid matter was removed from the yellowish extract (ULE) by filtration through a cotton pad. The concentrated green seaweeds extract (ULE 1) was obtained after the water evaporation at 60 °C (from 400 mL to 150 mL).

Synthesis of ZnO@C composites. Two hydrothermal synthesis routes, i.e. (*i*) one-pot synthesis (ZnO@C **1**, ZnO@C **1**-1) and (*ii*) two-steps synthesis (ZnO@C **2**) for ZnO@C composites were applied.

One-pot synthesis. 4.39 g (20 mmol) $Zn(CH_3COO)_2{\cdot}2H_2O$ were dissolved in 150 mL of green seaweeds extract (ULE for ZnO@C **1**, respective ULE 1 for ZnO@C **1**-1). A stoichiometric quantity of 1.60 g (40 mmol) NaOH was added to the resulted solution under stirring. The resulting mixture was magnetically stirred for 15 min at room temperature and then the reaction mixture was transferred into a hydrothermal reactor (Hydrothermal Autoclave Reactor CIT-HTC230-V200) and kept in an oven for 4 h at 180 °C. The light grey, respective grey powders were filtered off and washed with water.

Two-steps synthesis (ZnO@C **2**). 150 mL ULE were kept in a hydrothermal reactor for 4 h, at 180 °C. After cooling, the resulted suspension of black particles in a yellow-brown solution was ultrasonically treated (MRC D80H ultrasonic bath) for 15 min and then 4.39 g (20 mmol) $Zn(CH_3COO)_2{\cdot}2H_2O$, respective 1.60 g (40 mmol) NaOH were added successively. The mixture was magnetically stirred for 15 min, at room temperature and then the reaction mixture was transferred into the hydrothermal reactor, which was kept in an oven for 4 h at 180 °C. The grey powder was filtered off and washed with water.

Hydrothermal synthesis of ZnO nanopowders. 4.39 g (20 mmol) $Zn(CH_3COO)_2{\cdot}2H_2O$ were added to 150 mL of ULE (ZnO **1**), respective of water (ZnO–P **1** and ZnO–P **2**). A stoichiometric quantity of NaOH was added to the Zn^{2+} solution under stirring. The reaction mixture was magnetically stirred for 15 min at room temperature and then was transferred into a hydrothermal reactor, which was kept in an oven for 4 h at 80 °C (ZnO **1** and ZnO–P **2**), respective 180 °C (ZnO–P **1**). The obtained white powders were filtered off and washed with water.

Synthesis of ZnO nanopowders by chemical precipitation. 4.39 g (20 mmol) of $Zn(CH_3COO)_2{\cdot}2H_2O$ were added in 150 ml ULE (ZnO **2**), respective water (ZnO–P **3**). After the dissolution of zinc acetate, 1.60 g (40 mmol) of NaOH were added and then the reaction mixture was heated for 2 h, at 80 °C, under magnetic stirring. The resulted white powder was filtered off and washed with water.

2.3. Characterization of nanopowders

The powders were investigated by X-ray diffraction (XRD) performed on a Rigaku Miniflex 2 diffractometer with Ni filtered CuKα radiation, in the range of 2θ, 20–70°, scan rate of 2°/min and a step of 0.02°. The powders morphology was analyzed using a Tescan Vega 3LMH scanning electron microscope (SEM) and the particles dimension was determined by using the Vega3 software, at least 50 particles being measured to determine mean size value and standard deviation (SD). The UV–visible diffuse reflectance spectra (DRS) of powders were recorded in the range of 220–850 nm, on a Jasco V 550 spectrophotometer with an integrating sphere using MgO as the reference. The FTIR spectra were recorded on Agilent Cary 630 FTIR spectrometer with a ZnSe ATR, in the wave number range of 4000–650 cm^{-1}. The photoluminescence (PL) spectra were measured on a Jasco FP-6500 spectrofluorometer. The thermogravimetric (TG) and differential thermal analysis (DTA) curves were recorded using a Netzsch Regulus STA 2500 equipment over a temperature range of 30–1000 °C and a heating rate of 10 °C/min. The measurements were carried out in synthetic air using alumina crucibles. The total organic carbon (TOC) content of the ZnO@C samples was determined by combustion method with the Solid Sample Module (SSM-5000A) for the Shimadzu TOC analyser. The photocatalytic properties of ZnO nanopowders were estimated by monitoring of the degradation of Congo red azo dye using the Jasco V 550 spectrophotometer (200–900 nm). The FTIR spectrum of ulvan obtained from *Ulva lactuca* was recorded after extraction and purification [27] on a Bruker Tensor 27 spectrometer using KBr pellets technique, in the wave number range of 4000–400 cm^{-1}.

2.4. Photocatalytic properties of zinc oxide nanopowders

The photocatalytic properties of ZnO@C composites, in comparison with ZnO powders, were tested in the degradation of CR azo dye, following the procedure previously published [28,29]. In brief, the photocatalyst powders were dispersed in the CR solutions placed in Pyrex vessels and the mixtures were magnetically stirred for 30 min in dark to reach the equilibrium of adsorption – desorption process. Afterwards, the mixtures were irradiated perpendicularly to the surface by a visible light source (45 W mercury-vapor lamp, 815 lx) which spectrum, measured with a HR4000CG-UV-NIR high-resolution spectrometer (Ocean Optics), matches with the solar spectrum, respective with a shortwave UV (254 nm) Analytik Jena lamp (2 × 15 W, 450 lx), fixed at 20 cm. The suspensions were magnetically stirred for another 2 h. The samples were collected at regular intervals, filtered and centrifugated, and the absorbance was measured by a Jasco V 550 spectrophotometer.

3. Results and discussion

3.1. Characterization of ZnO-based nanopowders

3.1.1. X-ray diffraction

The crystalline phase was identified by X-ray diffraction (Fig. 1), which confirmed the formation of ZnO with the hexagonal wurtzite structure ($P6_3mc$ space group, ICDD 00-036-1451) and no characteristic peaks of any impurity were identified in the XRD patterns of ZnO@C. The presence of carbon was not identified in XRD patterns, probably because of low quantities and its amorphous nature.

For comparison, in the XRD patterns of the ZnO samples obtained in ULE, either by hydrothermal method (ZnO **1**) or chemical precipitation (ZnO **2**) obtained at 80 °C, an additional peak of very low intensity assigned to (0 2 1) diffraction plane of hydrozincite ($Zn_5(CO_3)_2(OH)_6$, ICDD 00-019-1458) [30] can be observed in agreement with literature data on ZnO obtained by precipitation with organic bases [30–32]. The hydrozincite phase was also identified in the XRD patterns of ZnO powders obtained at 80 °C (ZnO–P **2** and ZnO–P **3**) by both hydrothermal and chemical precipitation method.

The crystallites size of ZnO was determined from the XRD data using Rigaku PDXL software based on Scherrer's equation from the most intense diffraction peak (1 0 1). The average crystallite size of ZnO was calculated as 29.98 (ZnO@C **1**), 31.34 (ZnO@C **1**-1), and 30.34 nm (ZnO@C **2**) for ZnO@C samples, the increase for ZnO@C **1**-1 being correlated with a higher C content. Lower values of 24.05 nm (ZnO **1**), respective 23.08 nm (ZnO **2**) were calculated for the average crystallite size of ZnO samples. The crystallites size for pristine ZnO samples was calculated as 35.86 nm (ZnO–P **1**), 31.43 nm (ZnO–P **2**), and 31.67 nm (ZnO–P **3**), similar values being obtained for powders synthesized at the same temperature (80 °C), regardless of the synthesis method. As expected, a higher synthesis temperature led to a higher crystallinity and an increase of the crystallites dimension was calculated for ZnO–P **1** sample; the increase of nanoparticles average size with reaction temperature of hydrothermal treatment has been evidenced by other studies for a variety of nanomaterials [33]. The lower values for ZnO-based powders obtained in ULE compared to the pristine powders are due to the presence of phycocolloids in ULE.

Comparing the XRD patterns of ZnO@C composites with that of ZnO–P **1**, a difference between intensity ratio of the three most intense peaks can be noted, which implies a different distribution of atoms between the three diffraction planes. Slight differences can be observed for the peaks position (2θ values) and very similar values for the interplanar distance, d, which can prove that C atoms were not inserted in the ZnO lattice.

3.1.2. Scanning electron microscopy

The morphology of ZnO@C samples was studied by SEM (Fig. 2), which revealed the formation of microspheres with diameters between 104 and 320 nm and a mean diameter of 207 ± 54 nm for ZnO@C **1**, 82–313 nm and 192 ± 51 nm mean diameter for ZnO@C **1**-1, respective 92–292 nm and 149 ± 41 nm for ZnO@C **2** (magnification 50k). Comparing the particles dimension for ZnO@C **1** and ZnO@C **2** samples obtained in ULE with the same concentration, it can be seen that they are in similar value ranges, but the mean diameter is lower for ZnO@C **2** obtained by the two steps method. The ULE concentration was higher in the synthesis of ZnO@C **1**-1, meaning that both biochar particles and phycocolloids concentrations are higher; under the effect of the two components of ULE, the particle dimensions are similar to those ZnO@C **1**, despite the different chemical composition. In comparison with pristine ZnO obtained in similar conditions, the particles shape of ZnO@C composites seem to be more regular and spherical. The results revealed that the aggregates shape and dimension are influenced by the presence and concentration of ULE, which is both a source of biochar and a template for ZnO particles formation.

The one-pot synthesis of ZnO@C **1** involves the obtaining of C particles simultaneously with ZnO nanopowder. The two-steps synthesis of

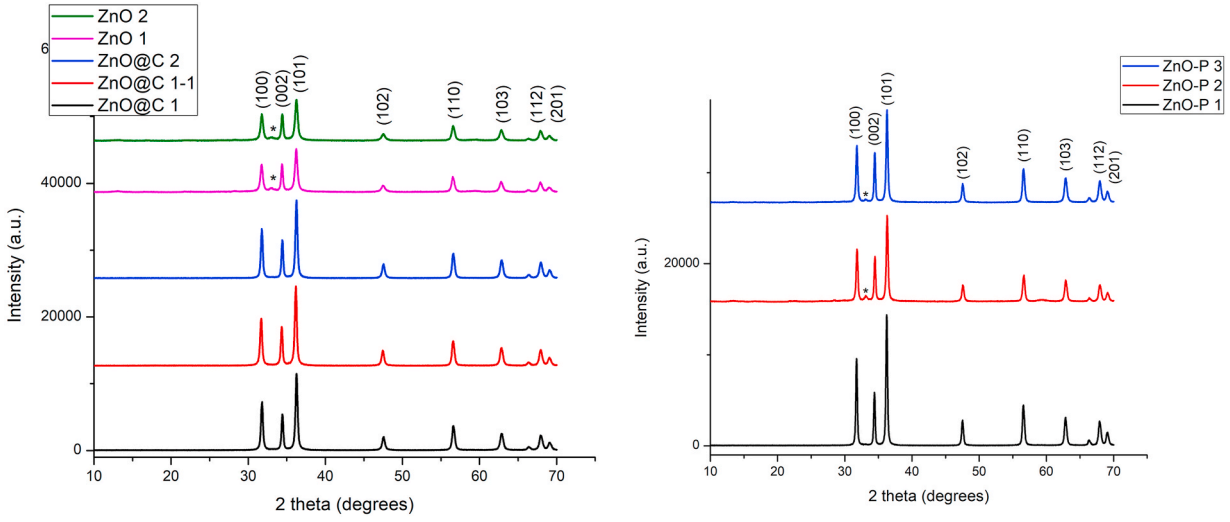

(a) (b)

Fig. 1. XRD diffraction patterns for ZnO-based nanopowders: a). Obtained in ULE; b). Pristine.

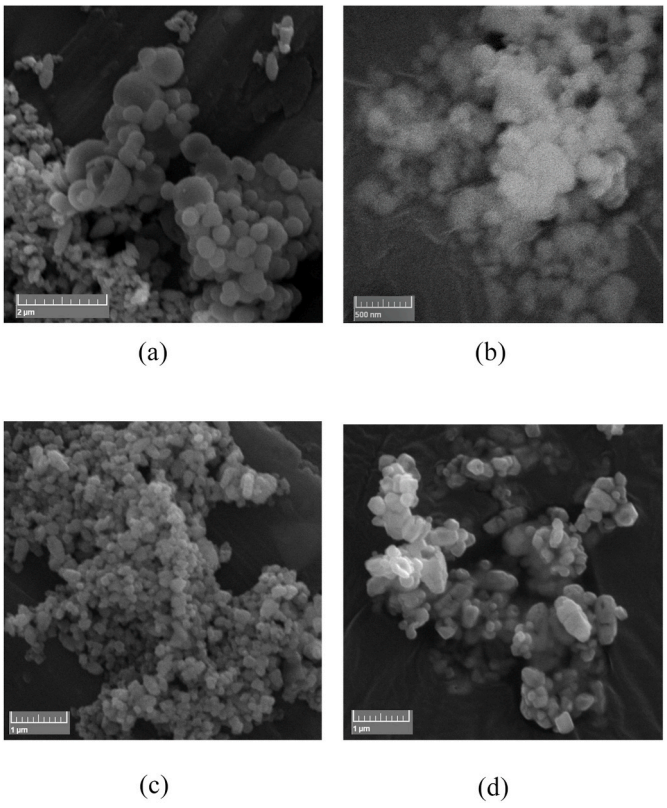

Fig. 2. SEM images for ZnO@C **1** (a, SEM magnification 20.0 kx), ZnO@C **1**-1 (b, SEM magnification 50.0 kx), and ZnO@C **2** (c, SEM magnification 25.0 kx) in comparison with pristine ZnO (d, SEM magnification 25.0 kx) obtained in similar conditions.

ZnO@C **2** consists in the hydrothermal degradation of biomolecules from ULE and the nanobiochar obtaining, in the first step, followed by the synthesis of ZnO in the second step. The synthesis of carbon spheres by hydrothermal treatment is presumed to have taken place in the first step as it was reported by other authors [14,34]. The as-prepared carbon spheres can serve as a template for ZnO particles. It was demonstrated [14] that the precursor $Zn(OH)_2$ preferentially nucleates at the carbon sphere template. A lower dimension for the nanocomposite aggregates was determined for the ZnO@C composite obtained by the two-steps method. Most probably, due of the existence of biochar particles obtained in the first stage, a lot of them acted as nucleation centers, which led to smaller aggregates. The almost spherical shape of particles, evidenced especially for ZnO@C **1** sample, can be an indication for the presence of surfactants, most probably the polysaccharides like ulvan, which can be preserved in the reaction medium due to its high thermal stability until 200 °C [24]. The increase of ULE concentration had the consequence of obtaining a more homogeneous powder for ZnO@C **1**-1 sample, with dimensions of the aggregates in a narrower range.

3.1.3. *Diffuse reflectance spectroscopy*

UV–vis diffuse reflectance spectroscopy (DRS) has been used to study the optical properties of ZnO-based samples. Thus, the UV–vis absorption spectra of ZnO@C composites (Fig. 3) in comparison with those of ZnO samples obtained in ULE, respective pristine ZnO obtained in similar conditions, were performed.

It can be observed from Fig. 3 that all studied powders have strong absorption in the range of 300–400 nm in UV domain, the main difference between samples being in visible domain. Therefore, the light absorption of ZnO@C nanocomposites is stronger than that of ZnO nanopowders, extending the absorption range of the samples to the visible light region. The absorption of visible light is due to the biochar and it was demonstrated that the visible light absorption increases with an increase in carbon content [15,35].

By comparing the UV spectra of ZnO-based powders, it can be seen that the spectrum shape depends on the ZnO obtaining conditions. Accordingly, the intense band which appears in the spectra of ZnO obtained at 80 °C, regardless of the synthesis method, is split in two bands in spectra of nanopowders obtained by hydrothermal method at 180 °C, including ZnO@C composites. The maxima of absorption for these bands are situated at 329 and a shoulder at about 356 nm (ZnO@C **1**), 330 and 361 nm (ZnO@C **1**-1), 338 and 358 nm (ZnO@C **2**), respective 339 and 365 nm (ZnO–P **1**). It is known that the direct valence band of the wurtzite ZnO structure can be split into three states, commonly called A, B, and C sub-bands, due to crystal field and spin-orbit interactions [36, 37].

The values of optical band gap energy (E_g) were calculated from UV–vis diffuse reflectance spectra by using the Kubelka-Munk and Tauc models. Based on the theory of Kubelka and Munk [38], the DRS were transformed to the corresponding absorption spectra by applying the Kubelka−Munk function [39]. Based on Tauc equation for a direct band gap, the determination the point of the extrapolation on the abscissa of Tauc plot ($(\alpha h\nu)^2$ versus $h\nu$) linear part which gives the band gap energy value [40].

The E_g values determined by Kubelka−Munk equation are indicated in Fig. 3 (inserts). The results are very close, in the range of 3.241–3.282 eV. The factor that seems to influence the value of band gap energy is the

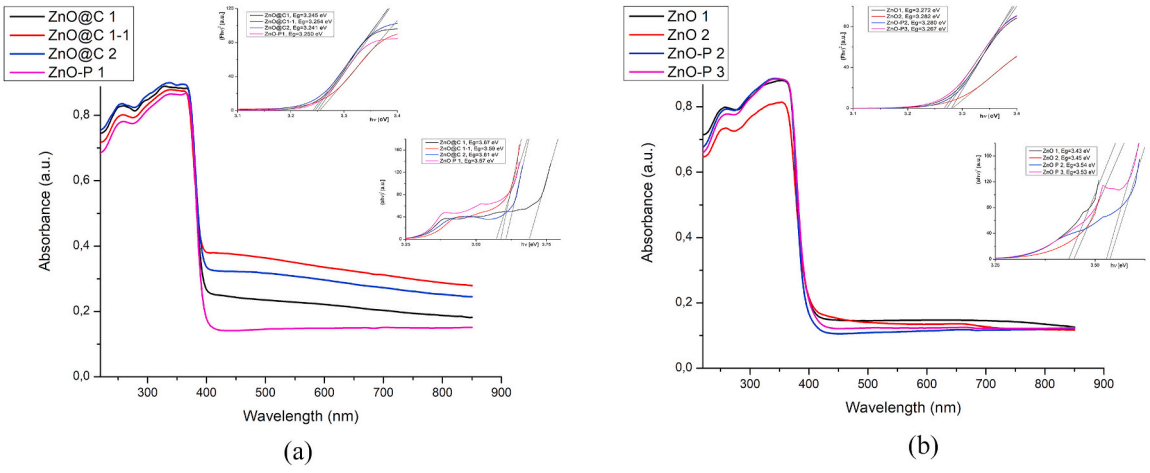

Fig. 3. UV–vis spectra of ZnO@C (a) and ZnO (b) nanopowders obtained in ULE in comparison with ZnO nanopowders obtained in aqueous solution in similar conditions, with the Kubelka-Monk absorption curves (up) and Tauc plots (down) inserted.

temperature in the synthesis method. Namely, a lower value of 3.25 eV was determined for ZnO particles obtained by hydrothermal method in aqueous solution at high temperature, which also have the higher crystallites size. The modification of the synthesis medium (ULE *vs.* aqueous solution) seems not to influence the value of E_g because only very small variations were observed for the ZnO@C and ZnO nanopowers obtained in ULE. The presence of biochar induced small variation for *Eg* values. The results obtained by Tauc model considering direct allowed transitions (Fig. 3, inserts) show that the band gap slightly increased with the increasing on biochar content. An explanation can be the increasing of ZnO electric surface charge within the composite due to the introduction of carbon. This electronic interaction between ZnO and C can be a source of changes in electron-hole pair formation during the irradiation and more photons would be expected to be absorbed and utilized in photocatalytic reactions [15]. The slight differences between pristine and capped nanopowders can be due to the additional energy levels that may appear in ZnO obtained ULE.

3.1.4. Photoluminescence spectroscopy

Photoluminescence spectroscopy was used to study the optical properties of ZnO@C composites, in comparison with ZnO nanopowders obtained in ULE. The PL spectra (Fig. 5) were measured for 360 nm excitation wavelength.

The first important observation which can be seen in Fig. 4 implies the lower intensity of emission bands in the spectra of ZnO@C samples. This behavior can be associated with the heterojunction constituted by ZnO and carbon, thus reducing the efficiency of recombination of photogenerated carriers and the emission intensity [14]. The ratio between intensity of emission bands in UV and visible domain is higher for ZnO@C composites, due to a extremely low intensity of broad bands situated in visible at about 550 nm. It is known that the intensity ratio between the UV and visible regions is important for characterization the emission purity of samples. It can be concluded that the amorphous carbon can reduce the number of defect centers and passivate the surface of ZnO, protecting ZnO from photocorrosion [3]. The PL spectra of ZnO-based samples exhibit a sharp peak around 387 nm in the violet domain, which can be assigned to lattice defects, and a wide band in the visible domain, with maximum at 554 nm, which are assigned to the near band edge and defect-related emissions respectively [3]. Another low intensity emission band can be found around 467 nm in the blue domain and can be assigned to the surface defects [41].

Based on PL spectra, ZnO@C nanocomposites are expected to have better photocatalytic activity due to inhibition of electron–hole recombination.

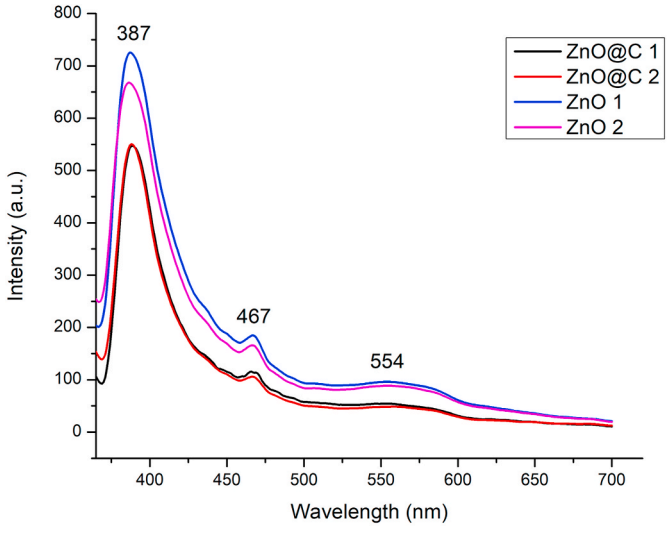

Fig. 4. PL emission spectra of ZnO-based samples excited with 360 nm wavelength radiation.

3.1.5. FTIR spectroscopy

The ZnO@C and ZnO nanopowders were analyzed by ATR-FTIR spectroscopy in 4000–650 cm^{-1} domain in order to identify the presence of capping molecules and impurities.

The FTIR spectra for ZnO@C composites are quite similar (Fig. 5.a), presenting a very week broad band centered at 3380 cm^{-1}, which is assigned to O–H groups associated by hydrogen bonding, the low intensity of bands being corelated with the low hydrophilicity of nanocomposites. Another more intense broad band can be found in the 2000–650 cm^{-1} domain, whose shape and width suggested that it was the result of overlapping several bands, which are not well defined, attributed to the functional groups formed in the decomposition of biomolecules. The 2000-650 cm^{-1} domain is characteristic to C═C, C–O and C═O bonds. Similar FTIR spectra with a broad band at wavenumbers under 2000 cm^{-1}, have been reported for biochar obtained from different sources [42]. A very weak broad band in the range of 1150–650 cm^{-1} is also detectable for ZnO–P **1**, probably originating from acetate anion used in the synthesis of the sample.

The spectra of ZnO powders obtained in ULE extract are very similar with those of ZnO obtained in aqueous solutions (Fig. 5.b). The ZnO samples spectra indicate the presence of carbonate group in hydrozincite, as the XRD patterns revealed, and acetate ion. Thus, the vibrations at 704, 831, 1390, 1502, and 1554 cm^{-1} in ZnO **1** spectrum, respective at 704, 835, 1386, 1502, and 1554 cm^{-1} in ZnO **2** spectrum, correspond to the bending vibration of CO_3^{2-}; the bands situated at 1386 and 1502 cm^{-1} can also be assigned to the presence of the acetate ions [30]. The bands from 1044 cm^{-1}, 1226 and 1248 cm^{-1} in ZnO **1** and ZnO **2** can be assigned to the stretching vibration of C–O bonds, respective to the S–O bonds from sulfate groups of ulvan [18,43]. The differences between the spectra of ZnO **1** and ZnO **2** samples, respective pristine ZnO samples obtained in similar conditions, as they can be seen in Fig. 5.b, consist in the bands situated at 1226 and 1248 cm^{-1}, thus the presence of ulvan as capping agent. The weak, broad band at 3324 (ZnO **1**), respective 3313 cm^{-1} (ZnO **2**) can be assigned to –OH groups associated by hydrogen bonding.

Although the FTIR-ATR spectroscopy is a proper technique for identifying the polysaccharides from seaweeds, as it was demonstrated by Gómez-Ordóñez and Rupérez [18], a few of the bands assigned to ulvan (Fig. 5.c), the major polysaccharide in *Ulva lactuca*, are overlapped by the bands assigned to carbonate ion, the bands in 1200–1300 cm^{-1} domain being those which can be clearly assigned to ulvan [18,27,43]. A further thermal treatment of as-obtained nanopowders should remove a part of capping agents and hydrozincite traces, as it was shown by Ishwarya et al. [44], but the presence of these species can improve the powders' properties.

The presence of organic compounds, as the FTIR spectra of ZnO@C composites demonstrated, is also confirmed by the determination of total organic carbon (TOC). The TOC content of ZnO@C samples was 1.45% (ZnO@C **1**), 2.32% (ZnO@C **1**-1), respective 0.77% (ZnO@C **2**). It can be observed that, starting from the same concentration of the ULE, the largest amount of organic carbon was determined by the one-pot method. In TOC content are included both carbon from capping agents and amorphous carbon. Considering the powders' color confirmed by the electronic spectra in visible domain, a higher quantity of amorphous carbon is supposed to be found in ZnO@C **2** compared to ZnO@C **1**, although the TOC content of ZnO@C **2** is lower. This assumption is reasonable because the reaction time for ULE in the synthesis of ZnO@C **2** is longer and it is expected that the biomolecules to be degraded in time to amorphous carbon more than in the synthesis of ZnO@C **1**, but the experimental evidences can not make a clear distinction between the existence forms of carbon in Zn@C composites. By increasing the concentration of ULE, ZnO@C composites with a higher concentration of TOC can be obtained. The results are well correlated with the thermal analysis and the absorption intensity in electronic and FTIR spectra of

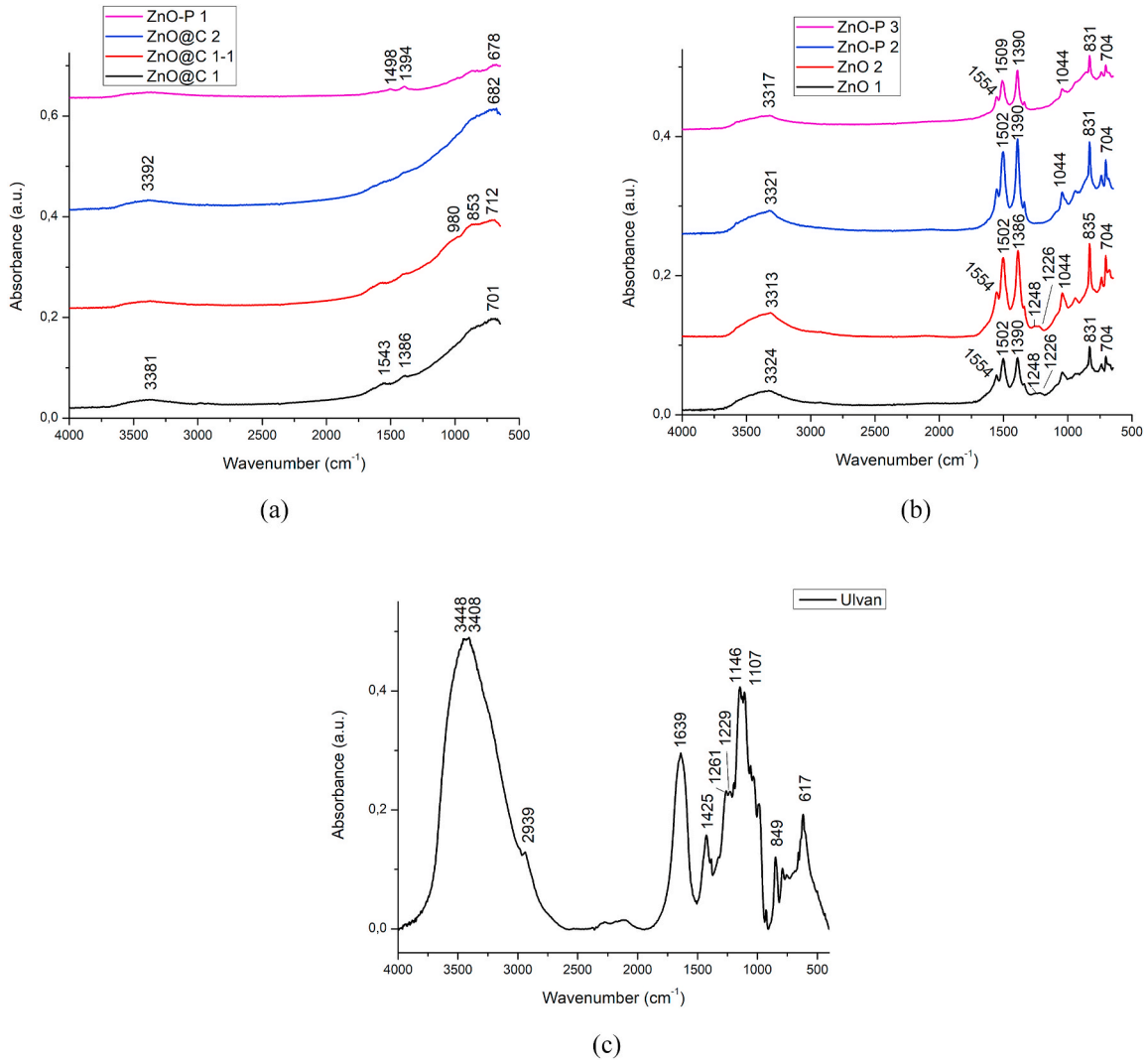

Fig. 5. FTIR spectra for: ZnO@C composites (a) and ZnO nanopowders (b) in comparison with ZnO–P samples; ulvan [27] (c).

composites.

3.1.6. Thermal analysis

The thermal decomposition of ZnO@C nanocomposites was studied in order to obtain information about the chemical composition and thermal stability (Fig. 6).

In the first step, a mass loss of 0.17% (ZnO@C **1**), 0.19% (ZnO@C **1**-1), respective 0.14% (ZnO@C **2**) was determined in a similar temperature range (up to 120–125 °C) for all samples. In this step, the physiosorbed water molecules are removed, the small amount of water in the samples being in concordance with the hydrophobic character of composites suggested by FTIR spectra. Although a quite similar thermal behavior can be noted for all three samples, a few differences can be identified at higher temperatures. Thus, in the thermal decomposition of ZnO@C **2** sample, two exothermic events occur in the 125–307 °C temperature range, which correspond to the caping agents' decomposition and carbon burning with a total mass loss of 2.50%. [28,45]. Unlike the case of ZnO@C **2**, for ZnO@C samples obtained by one-pot method (ZnO@C **1**, ZnO@C **1**-1) the two events are overlapped and only one step can be seen in each DTA curve. The exothermic events occur above 120 °C with a mass loss of 2.72% and 3.49% for ZnO@C **1** and ZnO@C **1**-1, respectively. For ZnO@C **1** the overlap is obvious and DTG curve also suggests the existence of two stages. Another difference consists in the temperature of the maximum weight loss rate in the second step, which increased from ZnO@C **1** to ZnO@C **2**. These differences may be due tot the different ratio of capping molecules to amorphous carbon in ZnO@C **1** and ZnO@C **2** samples, the two forms of carbon having different behavior in thermal degradation. For ZnO@C **1**-1 the two stages in the second step cannot be distinguished in TG curve, and the shape of DTG curve is changed, with a maximum of weight loss rate at 335 °C and a shoulder at 265–270 °C; its behavior is due to a higher content of amorphous carbon, as other experimental data confirmed.

3.2. Photocatalytic properties

The degradation of Congo Red (CR) in aqueous solutions was performed to assess the photocatalytic properties of ZnO@C composites in comparison with capped ZnO and pristine ZnO samples. CR is a representative diazo compound, which is suspected to produced toxic effects and interfered with photosynthesis in aquatic medium [46]. The discoloration of a CR solution signifies the breaking of azo bonds which are responsible for the CR color.

A concentration of 30 mg/L CR and a ratio of 0.05 g catalyst/100 mL CR solution were used. In our previous studies we demonstrated that the selected conditions are convenient to compare the photocatalytic properties of inorganic materials [28]. The stability of the dye against irradiation in the visible and UV light was estimated by the same

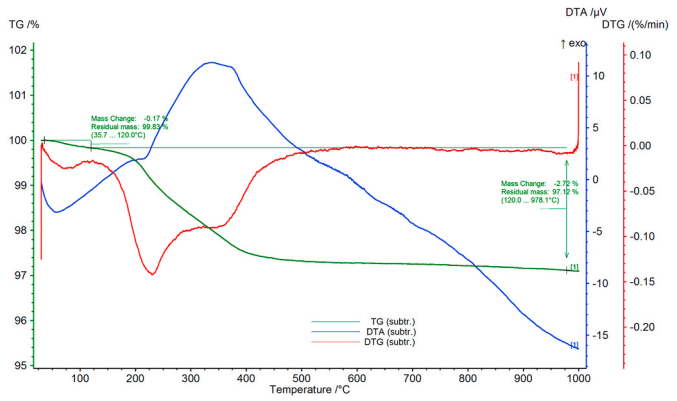

(a)

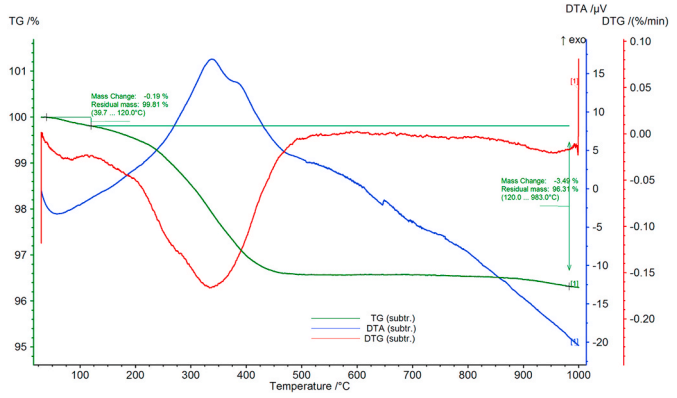

(b)

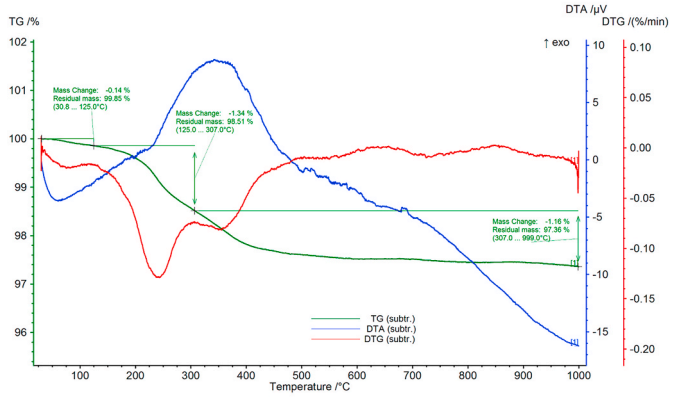

(c)

Fig. 6. TG, DTG and DTA curves for ZnO@C **1** (a), ZnO@C **1**-1 (b), and ZnO@C **2** (c).

procedure, but in the absence of the photocatalyst. The experiments were carried out under either UV or visible irradiations. The good photocatalytic activity determined us to test a higher concentration of CR (45 mg/L) with the same ratio of 0.05 g catalyst/100 ml CR solution.

The photodegradation of CR was estimated by C_t/C_i ratio (where C_t and C_i are the concentration of CR at certain time, *t,* and initial concentration, respectively). The efficiency of ZnO nanopowders was measured by the photocatalytic activity (*PA*):

$$PA = \frac{C_i - C_t}{C_i} x100 = \frac{A_i - A_t}{A_i} x100 \quad (1)$$

where A_i, A_t are the absorbance value for CR solutions measured at 497 nm for a certain time, *t*, and the initial concentration (based on Lambert – Beer law) [47].

The results of photocatalytic experiments (Fig. 7) demonstrated a good photocatalytic activity for ZnO@C composites. The photocatalytic activity is improved by the UV irradiation, the extent of increasing being dependent on the nature of the powder. As expected, the photocatalytic activity decreased with the increasing of CR concentration, but the decrease of PA is not high compared to the variation of concentration (increase by 50%), the photocatalyst powders being effective at this concentration as well. The same observations are also for ZnO samples. In absence of any photocatalyst, the concentration of CR under the visible and UV irradiation remained almost constant for 120 min, with a very low decrease of 3.07% under visible [48], respective 1% under UV treatment.

The photocatalytic activity of ZnO@C samples is comparable with that of ZnO nanopowders obtained in ULE, being slightly superior to pristine ZnO obtained in the similar conditions; the highest photocatalytic activity was determined for ZnO@C **2** sample, obtained by a two-stages method and assumed to have a higher carbon and lower capping molecules concentration compared to ZnO@C **1**. Furthermore, in the experiment carried out in 30 mg/L CR solution under UV illumination, the photocatalytic activity of ZnO@C **2** sample was highest. The comparison of photocatalytic activity revealed that there are some differences depending on the synthesis method. So, the pristine powders obtained by hydrothermal method at lower temperature and by chemical precipitation have higher photocatalytic activity and the values of PA are comparable. The same trend is maintained for ZnO obtained in green seaweeds extract, the samples denoted ZnO **1** and ZnO **2** having similar and high photocatalytic activity. Therefore, a high photocatalytic activity can be associated with the synthesis of ZnO particles at 80 °C by chemical precipitation or hydrothermal synthesis. A higher temperature (180 °C) for ZnO synthesis results in a higher crystallinity and lower photocatalytic activity. The combination of ZnO particles and biochar in composite materials led to an enhanced photocatalytic activity.

Despite the advantages of biochair presence in composites, the previous studies have shown that it is not a linear dependence between the chair content in a ZnO@C composite and its photocatalytic activity; namely, too much or too little carbon content decreased the photocatalyst performance, probably because of the increasing rate of separation efficiency of photogenerated carriers and the decreasing contact area of ZnO with the dye according to the carbon content [14]. In our study we confirmed this assertion, the highest photocatalytic activity being obtained for ZnO@C **2** sample, lower photocatalytic activities being determined for ZnO@C **1** and ZnO@C **1**-1 samples with lower, respective higher carbon quantities as it is suggested by UV–vis spectra corelated with thermal analysis and TOC determination. Comparing the two methods proposed for the obtaining of ZnO@C two-steps method led to a composite with better photocatalytic activity.

All ZnO-based powders have a good photocatalytic activity, the PA values after 120 min being between 80.76% and 92.40% (30 mg/L, visible), 83.81–91.89% (30 mg/L, UV), respective 72.03–89.45% (45 mg/L, visible).

In the electronic spectrum of CR in aqueous solution two absorption bands in UV domain can be found, in addition to the very intense band centered at 498 nm and assigned to the chromophore azo group. These bands are corelated with the transition of non-bonding and π molecular orbital electrons, and the decrease in intensity of those bands demonstrated the degradation of CR molecules, not only the breaking of azo bond.

In fact, the experiments were carried out in two consecutive conditions: the first one, included adsorption of CR onto nanopowders in the dark conditions for 30 min, while the second one was conducted under visible light, respective UV irradiation (λ = 254 nm) for 2 h [49]. Assuming that the adsorption – desorption equilibrium was established in 30 min of the experiment in dark conditions, the adsorption capacity

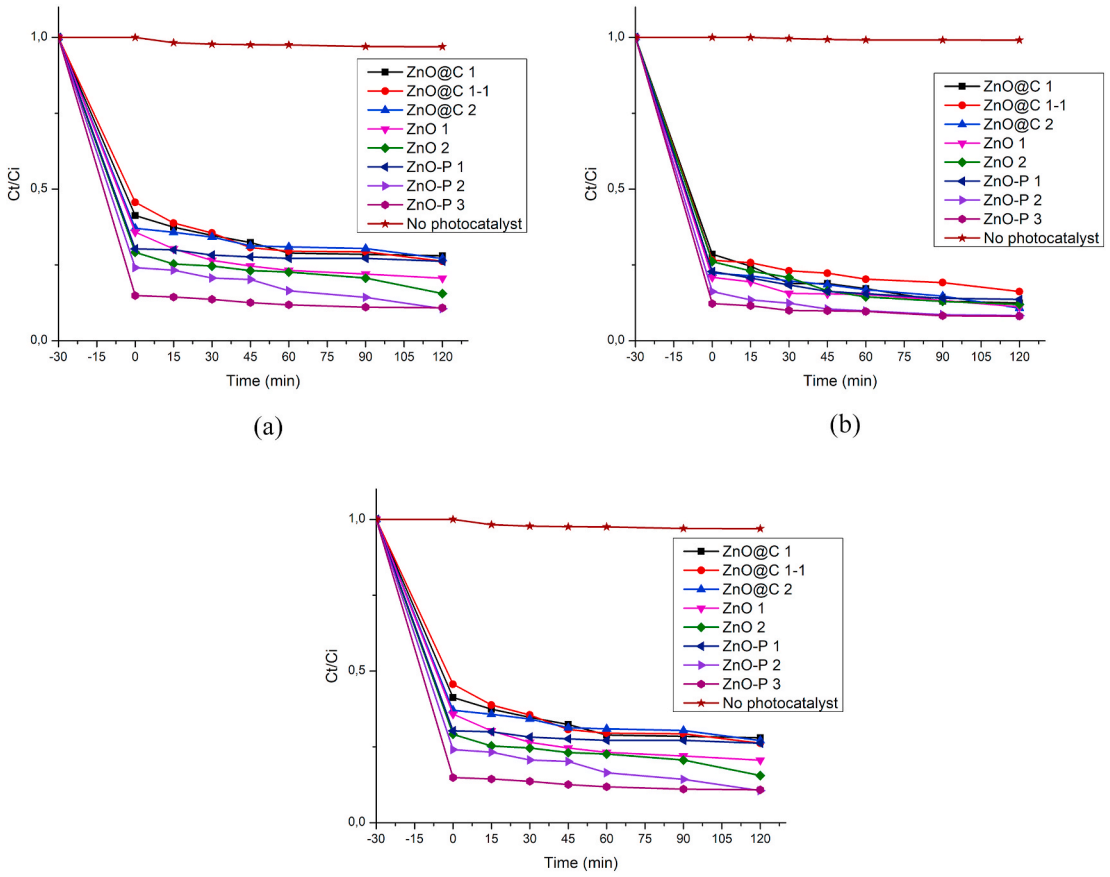

Fig. 7. The photocatalytic degradation curves of CR over ZnO@C and ZnO nanopowders: (a) 30 mg/L CR solution, under visible irradiation; (b) 30 mg/L CR solution, under UV irradiation; (c) 45 mg/L CR solution, under visible irradiation.

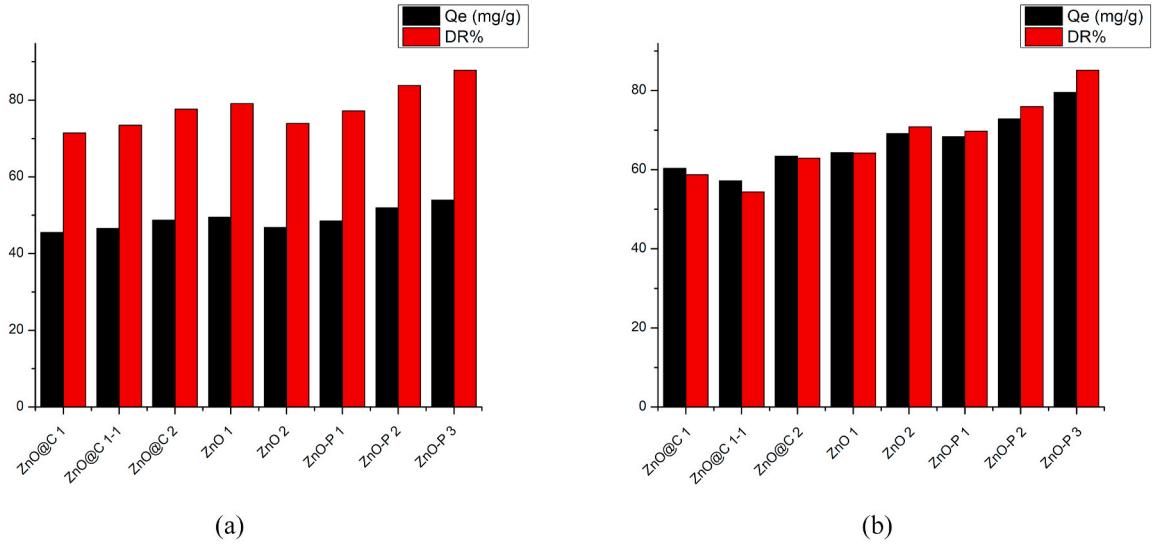

Fig. 8. The adsorption capacity, Q_e and the dye removal by adsorption, DR% for ZnO@C composites, in comparison with ZnO powders: (a) 30 mg/L CR; (b) 45 mg/L CR.

at equilibrium (Q_e, mg/g) and the dye removal (DR%) in dark were calculated as follows [50,51]:

$$Q_e = (C_i - C_e)\frac{V}{m} \quad (2)$$

$$DR\,\% = \frac{C_i - C_e}{C_0}\, x100 \quad (3)$$

where C_i is the initial dye concentration (mg/L), C_e (mg/L) is the equilibrium concentration, V is the volume of the dye solution (L) and m is the mass of adsorbent (g).

The adsorption capacity and the dye removal for ZnO@C composites, in comparison with ZnO powders, are represented in Fig. 8.

For the dye concentration of 30 mg/L, the adsorption capacity is high for all the samples. Considering the synthesis method, a better adsorption capacity was achieved for ZnO samples obtained by chemical precipitation. The lowest capacity was determined for ZnO samples obtained by hydrothermal synthesis at high temperature. The capping of ZnO particles also has the effect of lowering the adsorption capacity, probably through blocking of adsorption centers by caping molecules. The presence of biochar in ZnO@C composites improves the adsorption capacity of the samples. As expected, the quantity of adsorbed CR was higher in the experiment in which the CR solution of 45 mg/L was used.

A proper comparison between photocatalytic activity of the obtained ZnO-based nanopowders must involve systems in which the photocatalytic processes occur in similar conditions, namely the concentration of the dye, the ratio between the mass of photocatalyst and dye, the lighting source, the period of time of the process. In Table 1 we compare the present results with other obtained by our group and examples from literature.

The results can be discussed in terms of the influence of synthesis conditions on the photocatalytic properties of ZnO obtained by chemical precipitation, respectively hydrothermal synthesis. From the results presented in Table 1 for the photocatalysis in visible light, it can be seen that the increase of synthesis temperature, both in thermal decomposition and hydrothermal synthesis, had the effect of a decrease of photocatalytic activity, probably because of the particles dimension increasing. The presence of hydrozincite in ZnO nanopowder obtained by using the stoichiometric quantity of NaOH, under otherwise identical conditions, led to an increase of photocatalytic activity in comparison with the ZnO nanopowder obtained in stronger basic medium. The influence of ULE on the photocatalytic activity of ZnO nanopowders depends on the synthesis conditions. Thus, for the ZnO nanopowders obtained in ULE a lower PA was identified in comparison with pristine ZnO obtained in similar conditions. A similar behavior was obtained for ZnO nanopowder sensitized with anthocyanins [47]. For ZnO@C nanocomposites, a slightly higher or almost equal PA in comparison with pristine ZnO obtained in similar conditions can be observed. Under UV irradiation, the photocatalytic activity increased for almost all samples. A clear correlation between the determined TOC and the photocatalytic activity is difficult to understand due to the uncertainty in the estimation of the ratio between amorphous carbon and organic molecules. In order to combine successfully the high adsorption capacity of amorphous carbon with the photocatalytic activity of ZnO, a more comprehensive study of the relationship between carbon content and photocatalytic activity will be necessary.

Kinetic study. The Langmuir–Hinshelwood (L–H) kinetic mechanism was applied for the CR degradation over ZnO@C nanocomposites in comparison with ZnO, its suitability being demonstrated by many photocatalytic oxidation processes of various organic contaminants over semiconductors. The L-H model considers that the reactant is stronger adsorbed on the catalyst surface than the products [53–55]. Based on the low concentration of CR solutions (43, respective 64.6 μM), it can be considered that the photocatalytic degradation of CR follows the first order kinetics.

The dye concentration being micromolar, the L-H equation can be simplified to an apparent first-order equation, which can be written in a linearized form [53,55]:

$$\ln C_t = \ln C_0 - k_{app} \bullet t \quad (4)$$

where C_t is the concentration of the reactant (mg/L), C_0 – the initial

Table 1
Photocatalytic properties of ZnO-based samples in CR solutions.

Photocatalyst	Concentration of CR solution	Photocatalyst quantity/CR solution volume	Time/illumination	PA	Reference
ZnO nanopowder obtained by microwave-assisted hydrothermal process	16 mg/L	0.05 g/100 mL	60 min/100 W UV lamp (λ = 365 nm)	53.10%	[52]
Au/ZnO nanopowder				77.20%	
Ag/ZnO nanopowder				81.60%	
Pd/ZnO nanopowder				98.20%	
ZnO nanopowder obtained by chemical precipitation	30 mg/L	0.05 g/100 mL	120 min/45 W mercury lamp	86.40%	[47]
ZnO nanopowder sensitized with anthocyanins (chemical precipitation)				63.30%	
ZnO nanopowder functionalized with anthocyanins (chemical precipitation)				88.10%	
ZnO nanopowder obtained by calcination at 450 °C	30 mg/L	0.05 g/100 mL	120 min/45 W mercury lamp	82.79%	[28]
ZnO nanopowder obtained by calcination at 600 °C				77.11%	
ZnO nanopowder obtained by calcination at 800 °C				61.15%	
ZnO nanopowder obtained by hydrothermal method (ZnO–P **1**, 180 °C; ZnO–P **2**, 80 °C)	30 mg/L	0.05 g/100 mL	120 min/45 W (visible)	80.97% 91.06%	This study
ZnO nanopowder obtained by chemical precipitation				92.4%	
ZnO@C nanocomposites obtained in *Ulva lactuca* extracts (ZnO@C **1**, ZnO@C **1**-1, ZnO–C **2**)				80.76% 81.61% 81.81%	
ZnO nanopowders obtained in *Ulva lactuca* extract (ZnO **1**, ZnO **2**)				83.85% 91.21%	
ZnO nanopowder obtained by hydrothermal method (ZnO–P **1**, 180 °C; ZnO–P **2**, 80 °C)	30 mg/L	0.05 g/100 mL	120 min/2 × 15 W (UV, λ = 254 nm)	86.38% 91.73%	This study
ZnO nanopowder obtained by chemical precipitation				91.89%	
ZnO@C nanocomposites obtained in *Ulva lactuca* extracts (ZnO@C **1**, ZnO@C **1**-1, ZnO–C **2**)				87.56% 83.81% 89.28%	
ZnO nanopowders obtained in *Ulva lactuca* extract (ZnO **1**, ZnO **2**)				88.86% 88.04%	

Table 2
Kinetic parameters (k_{app}; experimental and calculated value of CR concentration after dark adsorption, C_0; coefficient of determination, R^2) for the photocatalytic degradation of CR dye with ZnO@C nanocomposites in comparison with ZnO nanopowders as catalysts (0–120 min).

Sample	$C_{0,\ exp.}$ (mg·L^{-1})	L – H simplified model		
		C_0 (mg·L^{-1})	k_{app} (min^{-1})	R^2
30 mg/L, visible				
ZnO@C **1**	7.79	7.42	0.0036	0.9368
ZnO@C **1–1**	8.53	8.51	0.0044	0.9481
ZnO@C **2**	9,00	9.48	0.0059	0.9704
ZnO–P **1**	8.07	7.80	0.0036	0.9368
ZnO **1**	7.42	7.31	0.0047	0.9898
ZnO–P **2**	6.94	6.02	0.0095	0.9287
ZnO **2**	5.63	5.83	0.0078	0.9372
ZnO–P **3**	7.14	6.33	0.0114	0.9487
30 mg/L, UV				
ZnO@C **1**	7.24	6.64	0.0072	0.9341
ZnO@C **1–1**	6.73	6.75	0.0042	0.98
ZnO@C **2**	5.64	5.92	0.0061	0.963
ZnO–P **1**	5.75	5.38	0.0045	0.9079
ZnO **1**	5.27	5.03	0.0051	0.9367
ZnO–P **2**	4.05	3.65	0.0058	0.9132
ZnO **2**	6.61	6.21	0.0070	0.9267
ZnO–P **3**	2.84	2.90	0.0037	0.9264
45 mg/L, visible				
ZnO@C **1**	14.83	13.90	0.0033	0.8562
ZnO@C **1–1**	14.77	16.42	0.0042	0.8521
ZnO@C **2**	13.31	13.13	0.0025	0.9396
ZnO–P **1**	10.84	10.67	0.0012	0.8638
ZnO **1**	12.84	11.46	0.0043	0.8644
ZnO–P **2**	8.59	9.12	0.0071	0.9719
ZnO **2**	10.43	10.21	0.0046	0.9310
ZnO–P **3**	5.25	5.18	0.0030	0.9391

value of the reactant concentration (after the adsorption in dark), k_{app} - the apparent first order rate constant, and t – the illumination time (min). The values of k_{app} and respectively C_0 , were determined the slope and the intercept of trend line in the linear fitting of the plot of ln C against time. The results are shown in Table 2.

The values from Table 2 revealed small differences between experimental and calculated values for C_0 and good values for R^2, which demonstrate that the kinetics of the photocatalytic process is a L-H-type.

By comparing the k_{app} values for ZnO@C samples with pristine ZnO, it can be seen that mostly higher values were determined for ZnO@C photocatalysts. The illumination with UV generally increased the k_{app} regardless of the nature of the samples. The increasing of CR concentration involves the decrease of k_{app}, which is in agreement with other reports [56]. The lowest values of R^2 for the CR concentration of 45 mg/L indicate that the L-H model fits better with diluted solutions, as was the case with the 30 mg/L CR concentration.

4. Conclusions

We report for the first time the use of *Ulva lactuca* aqueous extract as source of biomolecules and in the same time a precursor for nanobiochar for obtaining of ZnO@C nanocomposites. Two methods were developed for the synthesis of ZnO@C composites. In the two-step synthesis of ZnO@C composites, the carbon particles pre-exist in the synthesis medium and serve as growth centers for ZnO particles while the biomolecules act as surfactants, whereas in the one-pot synthesis the ZnO particles are initially obtained in absence of carbon growth centers but in the presence of larger amounts of phycocolloids and the capping organic molecules were subsequently degraded to biochar. These differences on the synthesis routes influenced the chemical composition and properties of the obtained nanocomposites. The XRD patterns confirmed the formation of wurtzite phase for ZnO in all samples. The PL spectra of ZnO@C composites can be correlated with their good photocatalytic activity. All samples obtained in the *Ulva lactuca* extract, either ZnO@C or capped ZnO powders exhibited high photocatalytic activities for CR anionic azo dye degradation after 120 min, which was in the 80–91% range, slightly higher in the case of the UV illumination (84–89%). The experimental results fit well with the Langmuir–Hinshelwood kinetic model, especially for the lower concentration of CR. The two-stages method hydrothermal synthesis is more suitable than one-pot method for obtaining ZnO@C composite materials, having in view the composition, morphology and photocatalytic properties.

Declaration of competing interest

The authors declare that they have no known competing financial interests or personal relationships that could have appeared to influence the work reported in this paper.

Acknowledgements

The authors are grateful to Dr. Luminita Lazar (National Institute for Marine Research and Development “Grigore Antipa”, Constanta, Romania) for the TOC determination.

C.M. and D.B. are grateful for the financial support of the Romanian UEFISCDI projects PCE no. 117/2022 (COMCONF).

References

[[1] H. Morkoç, Ü. Özgür, Zinc Oxide: Fundamentals, Materials and Device Technology, Wiley-VCH Verlag, Weinheim, 2009.
[2] A. Kołodziejczak-Radzimska, T. Jesionowsk, Zinc oxide—from synthesis to application: a review, Materials 7 (2014) 2833–2881, https://doi.org/10.3390/ma7042833.
[3] T. Chen, S. Yu, X. Fang, H. Huang, L. Li, X. Wang, H. Wang, Enhanced photocatalytic activity of C@ZnO core-shell nanostructures and its photoluminescence property, Appl. Surf. Sci. 389 (2016) 303–310, https://doi.org/10.1016/j.apsusc.2016.07.122.
[4] C.B. Ong, L.Y. Ng, A.W. Mohammad, A review of ZnO nanoparticles as solar photocatalysts: synthesis, mechanisms and applications, Renew. Sustain. Energy Rev. 81 (2018) 536–551, https://doi.org/10.1016/j.rser.2017.08.020.
[5] P. Basnet, D. Samanta, T.I. Chanu, J. Mukherjee, S. Chatterjee, Assessment of synthesis approaches for tuning the photocatalytic property of ZnO nanoparticles, SN Appl. Sci. 1 (2019) 633, https://doi.org/10.1007/s42452-019-0642-x.
[6] S. Agarwal, L.K. Jangir, K.S. Rathore, M. Kumar, K. Awasthi, Morphology-dependent structural and optical properties of ZnO nanostructures, Appl. Phys. A 125 (2019) 553, https://doi.org/10.1007/s00339-019-2852-x.
[7] R. Hong, T. Pan, J. Qian, H. Li, Synthesis and surface modification of ZnO nanoparticles, Chem. Eng. J. 119 (2006) 71–81, https://doi.org/10.1016/j.cej.2006.03.003.
[8] P. Chandrasekaran, G. Viruthagiri, N. Srinivasan, The effect of various capping agents on the surface modifications of sol–gel synthesised ZnO nanoparticles, J. Alloys Compd. 540 (2012) 89–93, https://doi.org/10.1016/j.jallcom.2012.06.032.
[9] H. Mirzaei, M. Darroudic, Zinc oxide nanoparticles: biological synthesis and biomedical applications, Ceram. Int. 43 (2017) 907–914, https://doi.org/10.1016/j.ceramint.2016.10.051.
[10] K.G. Sudha, S. Ali, G. Karunakaran, M. Kowsalya, E. Kolesnikov, M.P. Rajeshkumar, Eco-friendly synthesis of ZnO nanorods using *Cycas pschannae* plant extract with excellent photocatalytic, antioxidant, and anticancer nanomedicine for lung cancer treatment, Appl. Organomet. Chem. 34 (2020), e5511, https://doi.org/10.1002/aoc.5511.
[11] D.M. Cruz, E. Mostafavi, A. Vernet-Crua, H. Barabadi, V. Shah, J.L. Cholula-Díaz, G. Guisbiers, T.J. Webster, Green nanotechnology-based zinc oxide (ZnO) nanomaterials for biomedical applications: a review, J. Phys.: Materials 3 (2020), 034005, https://doi.org/10.1088/2515-7639/ab8186.
[12] J. de O. Primo, C. Bittencourt, S. Acosta, A. Sierra-Castillo, J.F. Colomer, S. Jaerger, V.C. Teixeira, F.J. Anaissi, Synthesis of zinc oxide nanoparticles by ecofriendly routes: adsorbent for copper removal from wastewater, Front. Chem. 8 (2020), e571790, https://doi.org/10.3389/fchem.2020.571790.
[13] Y. Tu, Z. Peng, J. Huang, X. Wu, L. Kong, Z. Liang, L. Yang, Z. Lin, Preparation and characterization of magnetic biochar nanocomposites via a modified solvothermal method and their use as efficient heterogeneous Fenton-like catalysts, Ind. Eng. Chem. Res. 59 (2020) 1809–1821, https://doi.org/10.1021/acs.iecr.9b04590.
[14] C. Jin, K. Zhu, Z. Jian, Y. Wei, L. Gao, Z. Zhang, D. Zheng, Influence of carbon content on photocatalytic performance of C@ZnO hollow nanospheres, Mater. Res. Express 5 (2018), 025001, https://doi.org/10.1088/2053-1591/aaa81d.
[15] H. Cai, D. Zhang, X. Ma, Z. Ma, A novel ZnO/biochar composite catalysts for visible light degradation of metronidazole, Separ. Purif. Technol. 288 (2022), 120633, https://doi.org/10.1016/j.seppur.2022.120633.

[16] N. Chausali, J. Saxena, R. Prasad, Nanobiochar and biochar based nanocomposites: advances and applications, J. Agric. Food Res. 5 (2021), 100191, https://doi.org/10.1016/j.jafr.2021.100191.
[17] Y.D. Chen, F. Liu, N.Q. Ren, S.H. Ho, Revolutions in algal biochar for different applications: state-of-the-art techniques and future scenarios, Chin. Chem. Lett. 31 (2020) 2591–2602, https://doi.org/10.1016/j.cclet.2020.08.019.
[18] E. Gómez-Ordóñez, P. Rupérez, FTIR-ATR spectroscopy as a tool for polysaccharide identification in edible brown and red seaweeds, Food Hydrocolloids 25 (2011) 1514–1520, https://doi.org/10.1016/j.foodhyd.2011.02.009.
[19] H. Dominguez, E.P. Loret, Ulva lactuca, A Source of troubles and potential riches, Mar. Drugs 17 (2019) 357, https://doi.org/10.3390/md17060357.
[20] A. Alves, R.A. Sousa, R.L. Reis, A practical perspective on ulvan extracted from green algae, J. Appl. Phycol. 25 (2013) 407–424, https://doi.org/10.1007/s10811-012-9875-4.
[21] Y. Pengzhan, Z. Quanbin, L. Ning, X. Zuhong, W. Yanmei, L. Zhi'en, Polysaccharides from *Ulva pertusa* (Chlorophyta) and preliminary studies on their antihyperlipidemia activity, J. Appl. Phycol. 15 (2003) 21–27.
[22] F. Rahimi, M. Tabarsa, M. Rezaei, Ulvan from green algae Ulva intestinalis: optimization of ultrasound-assisted extraction and antioxidant activity, J. Appl. Phycol. 28 (2016) 2979–2990, https://doi.org/10.1007/s10811-016-0824-5.
[23] M. Lahaye, E.A.C. Cimadevilla, R. Kuhlenkamp, B. Quemener, V. Lognone, Patrick Dion, Chemical composition and 13C NMR spectroscopic characterisation of ulvans from Ulva (Ulvales, Chlorophyta), J. Appl. Phycol. 11 (1999) 1–7.
[24] A. Alves, S.G. Caridade, J.F. Mano, R.A. Sousa, R.L. Reis, Extraction and physico-chemical characterization of a versatile biodegradable polysaccharide obtained from green algae, Carbohydr. Res. 345 (2010) 2194–2200, https://doi.org/10.1016/j.carres.2010.07.039.
[25] C. Matei, D. Berger, A. Dumbrava, M.D. Radu, E. Gheorghe, Calcium carbonate as silver carrier in composite materials obtained in green seaweed extract with topical applications, J. Sol. Gel Sci. Technol. 93 (2020) 315–323, https://doi.org/10.1007/s10971-019-05145-6.
[26] A. Dumbrava, D. Berger, C. Matei, M.D. Radu, E. Gheorghe, Characterization and applications of a new composite material obtained by green synthesis, through deposition of zinc oxide onto calcium carbonate precipitated in green seaweeds extract, Ceram. Int. 44 (2018) 4931–4936, https://doi.org/10.1016/j.ceramint.2017.12.084.
[27] A.M. Brezoiu, A.M. Prelipcean, D. Lincu, M. Deaconu, E. Vasile, R. Tatia, A. M. Seciu-Grama, C. Matei, D. Berger, Nanoplatforms for irinotecan delivery based on mesoporous silica modified with a natural polysaccharide, Materials 15 (2022) 7003, https://doi.org/10.3390/ma15197003.
[28] A. Dumbrava, D. Berger, G. Prodan, M. Badea, R. Olar, F. Moscalu, A. Diacon, A study on thermal degradation of zinc oxide nanopowders functionalized with anthocyanins, in correlation with their properties and applications, Appl. Phys. A Mater. Sci. Process. 124 (2018) 819, https://doi.org/10.1007/s00339-018-2227-8.
[29] A. Dumbrava, G. Prodan, D. Berger, M. Bica, Properties of PEG-capped CdS nanopowders synthesized under very mild conditions, Powder Technol. 270 (2015) 197–204, https://doi.org/10.1016/j.powtec.2014.10.012.
[30] J. Zhang, S. Wang, M. Xu, Y. Wang, B. Zhu, S. Zhang, W. Huang, S. Wu, Hierarchically porous ZnO architectures for gas sensor application, Cryst. Growth Des. 9 (2009) 3532–3537.
[31] S. Music, S. Popovic, M. Maljkovic, D. Dragcevic, Influence of synthesis procedure on the formation and properties of zinc oxide, J. Alloys Compd. 347 (2002) 324–332, https://doi.org/10.1016/S0925-8388(02)00792-2.
[32] R. Wahab, S.G. Ansari, Y.S. Kim, M.A. Dar, H.S. Shin, Synthesis and characterization of hydrozincite and its conversion into zinc oxide nanoparticles, J. Alloys Compd. 461 (2008) 66–71.
[33] Z.A. Zulkifli, K.A. Razak, W.N.W.A. Rahman, The effect of reaction temperature on the particle size of bismuth oxide nanoparticles synthesized via hydrothermal method, AIP Conf. Proc. (2018), 020007, https://doi.org/10.1063/1.5034538, 1958.
[34] C. Jin, C. Ge, Z. Jian, Y. Wei, Facile synthesis and high photocatalytic degradation performance of ZnO-SnO_2 hollow spheres, Nanoscale Res. Lett. 11 (2016) 526, https://doi.org/10.1186/s11671-016-1740-y.
[35] M. Vinayagam, S. Ramachandran, V. Ramya, A. Sivasamy, Photocatalytic degradation of orange G dye using ZnO/biomass activated carbon nanocomposite, J. Environ. Chem. Eng. 6 (2018) 3726–3734, https://doi.org/10.1016/j.jece.2017.06.005.
[36] Ü. Özgür, Y.I. Alivov, C. Liu, A. Teke, M.A. Reshchikov, S. Doğan, V. Avrutin, S. J. Cho, H. Morkoç, A comprehensive review of ZnO materials and devices, J. Appl. Phys. 98 (2005), 041301.
[37] A. Galdámez-Martinez, G. Santana, F. Güell, P.R. Martínez-Alanis, A. Dutt, Photoluminescence of ZnO nanowires: a review, Nanomaterials 10 (2020) 857, https://doi.org/10.3390/nano10050857.
[38] P. Kubelka, F. Munk, A contribution to the optics of pigments, Z. Technol. Phys. 12 (1931) 593–599.
[39] P. Makuła, M. Pacia, W. Macyk, How to correctly determine the band gap energy of modified semiconductor photocatalysts based on UV−Vis spectra, J. Phys. Chem. Lett. 9 (2018) 6814–6817, https://doi.org/10.1021/acs.jpclett.8b02892.
[40] J. Tauc, R. Grigorovici, A. Vancu, Optical properties and electronic structure of amorphous germanium, Phys. Status Solidi B 15 (1966) 627–637, https://doi.org/10.1002/pssb.19660150224.
[41] S. Repp, E. Erdem, Controlling the exciton energy of zinc oxide (ZnO) quantum dots by changing the confinement conditions, Spectrochim. Acta Mol. Biomol. Spectrosc. 152 (2016) 637–644, https://doi.org/10.1016/j.saa.2015.01.110.
[42] M.S. Reza, S. Afroze, M.S.A. Bakar, R. Saidur, N. Aslfattahi, J. Taweekun, A. K. Azad, Biochar characterization of invasive *Pennisetum purpureum* grass: effect of pyrolysis temperature, Biochar 2 (2020) 239–251, https://doi.org/10.1007/s42773-020-00048-0.
[43] V. Jaulneau, C. Lafitte, C. Jacquet, S. Fournier, S. Salamagne, X. Briand, M. T. Esquerre-Tugaye, B. Dumas, Ulvan, a sulfated polysaccharide from green algae, activates plant immunity through the jasmonic acid signaling pathway, J. Biomed. Biotechnol. (2010), 525291, https://doi.org/10.1155/2010/525291, 2010.
[44] R. Ishwarya, B. Vaseeharan, S. Kalyani, B. Banumathi, M. Govindarajan, N. S. Alharbi, S. Kadaikunnan, Mohammed N. Al-anbr, Jamal M. Khaled, Giovanni Benelli, Facile green synthesis of zinc oxide nanoparticles using Ulva lactuca seaweed extract and evaluation of their photocatalytic, antibiofilm and insecticidal activity, J. Photochem. Photobiol. B Biol. 178 (2018) 249–258, https://doi.org/10.1016/j.jphotobiol.2017.11.006.
[45] M.E. Brown, Handbook of thermal analysis and calorimetry, in: Principles and Practice, 1, Elsevier, Amsterdam, 1998, p. 172.
[46] M. Hernández-Zamora, F. Martínez-Jerónimo, Congo red dye diversely affects organisms of different trophic levels: a comparative study with microalgae, cladocerans, and zebrafish embryos, Environ. Sci. Pollut. Control Ser. 26 (2019) 11743–11755, https://doi.org/10.1007/s11356-019-04589-1.
[47] A. Dumbrava, D. Berger, G. Prodan, C. Matei, F. Moscalu, A. Diacon, Influence of synthesis route on the structure and properties of zinc oxide nanoparticles functionalized with anthocyanins from raw vegetable extracts, ECS J. Solid State Sci. Technol. 6 (2017) P870–P878, https://doi.org/10.1149/2.0311712jss.
[48] A. Dumbrava, D. Berger, G. Prodan, C. Matei, F. Moscalu, A. Diacon, The influence of Triton X-100 surfactant on the morphology and properties of zinc sulfide nanoparticles for applications in azo dyes degradation, Mater. Chem. Phys. 193 (2017) 316–328, https://doi.org/10.1016/j.matchemphys.2017.02.040.
[49] M.N. Rashed, M.A. Eltaher, A.N.A. Abdou, Adsorption and photocatalysis for methyl orange and Cd removal from wastewater using TiO2/sewage sludge-based activated carbon nanocomposites, Royal Soc. Open Sci. vol. 4 (2017), 170834, https://doi.org/10.1098/rsos.170834.
[50] C.H. Weng, Y.F. Pan, Adsorption of a cationic dye (methylene blue) onto spent activated clay, J. Hazard Mater. 144 (2007) 355–362, https://doi.org/10.1016/j.jhazmat.2006.09.097.
[51] A.H. Jawada, A.S. Abdulhameed, Mesoporous Iraqi red kaolin clay as an efficient adsorbent for methylene blue dye: adsorption kinetic, isotherm and mechanism study, Surface. Interfac. 18 (2020), 100422, https://doi.org/10.1016/j.surfin.2019.100422.
[52] N. Guy, M. Ozacar, The influence of noble metals on photocatalytic activity of ZnO for Congo red degradation, Int. J. Hydrogen Energy 41 (2016) 20101–20112, https://doi.org/10.1016/j.ijhydene.2016.07.063.
[53] M.A. Behnajady, N. Modirshahla, R. Hamzavi, Kinetic study on photocatalytic degradation of C.I. Acid Yellow 23 by ZnO photocatalyst, J. Hazard Mater. 133 (2006) 226, https://doi.org/10.1016/j.jhazmat.2005.10.022.
[54] B. Liu, X. Zhao, C. Terashima, A. Fujishima, K. Nakata, Thermodynamic and kinetic analysis of heterogeneous photocatalysis for semiconductor systems, Phys. Chem. Chem. Phys. 16 (2014) 8751, https://doi.org/10.1039/c3cp55317e.
[55] A. Dumbrava, D. Berger, C. Matei, G. Prodan, F. Aonofriesei, M.D. Radu, F. Moscalu, New composite nanomaterials with antimicrobial and photocatalytic properties based on silver and zinc oxide, J. Inorg. Organomet. Polym. Mater. 29 (2019) 2072–2082, https://doi.org/10.1007/s10904-019-01166-4.
[56] D.F. Ollis, Kinetics of photocatalyzed reactions: five lessons learned, Front. Chem. 6 (2018) 378, https://doi.org/10.3389/fchem.2018.00378.